XMM cluster survey: the build up of stellar mass in brightest cluster galaxies at high redshift

Article (Published Version)

The Astrophysical Journal, 718:23–30, 2010 July 20 doi:10.1088/0004-637X/718/1/23

THE *XMM* CLUSTER SURVEY: THE BUILD-UP OF STELLAR MASS IN BRIGHTEST CLUSTER GALAXIES AT HIGH REDSHIFT

J. P. Stott[1], C. A. Collins[1], M. Sahlén[2], M. Hilton[1,3], E. Lloyd-Davies[4], D. Capozzi[1], M. Hosmer[4], A. R. Liddle[4], N. Mehrtens[4], C. J. Miller[5], A. K. Romer[4], S. A. Stanford[6,7], P. T. P. Viana[8,9], M. Davidson[10], B. Hoyle[11], S. T. Kay[12], and R. C. Nichol[13]

[1] Astrophysics Research Institute, Liverpool John Moores University, Twelve Quays House, Egerton Wharf, Birkenhead CH41 1LD, UK; jps@astro.livjm.ac.uk
[2] The Oskar Klein Centre for Cosmoparticle Physics, Department of Physics, Stockholm University, AlbaNova, SE-106 91 Stockholm, Sweden
[3] Astrophysics and Cosmology Research Unit, School of Mathematical Sciences, University of KwaZulu-Natal, Private Bag X54001, Durban 4000, South Africa
[4] Astronomy Centre, University of Sussex, Falmer, Brighton, BN1 9QH, UK
[5] Cerro-Tololo Inter-American Observatory, National Optical Astronomy Observatory, 950 North Cherry Avenue, Tucson, AZ 85719, USA
[6] University of California, Davis, CA 95616, USA
[7] Institute of Geophysics and Planetary Physics, Lawrence Livermore National Laboratory, Livermore, CA 94551, USA
[8] Departamento de Matemática Aplicada da Faculdade de Ciências da Universidade do Porto, Rua do Campo Alegre, 687, 4169-007 Porto, Portugal
[9] Centro de Astrofísica da Universidade do Porto, Rua das Estrelas, 4150-762 Porto, Portugal
[10] SUPA, Institute of Astronomy, University of Edinburgh, Royal Observatory, Blackford Hill, Edinburgh, EH9 3HJ, UK
[11] Institute for Sciences of the Cosmos (ICCUB), University of Barcelona, Marti i Franques 1, Barcelona 08024, Spain
[12] Jodrell Bank Centre for Astrophysics, School of Physics and Astronomy, The University of Manchester, Manchester M13 9PL, UK
[13] ICG, University of Portsmouth, Portsmouth PO1 2EG, UK
Received 2009 December 11; accepted 2010 May 20; published 2010 June 24

ABSTRACT

We present deep *J*- and K_s-band photometry of 20 high redshift galaxy clusters between $z = 0.8$ and 1.5, 19 of which are observed with the MOIRCS instrument on the Subaru telescope. By using near-infrared light as a proxy for stellar mass we find the surprising result that the average stellar mass of Brightest Cluster Galaxies (BCGs) has remained constant at $\sim 9 \times 10^{11}\, M_{\odot}$ since $z \sim 1.5$. We investigate the effect on this result of differing star formation histories generated by three well-known and independent stellar population codes and find it to be robust for reasonable, physically motivated choices of age and metallicity. By performing Monte Carlo simulations we find that the result is unaffected by any correlation between BCG mass and cluster mass in either the observed or model clusters. The large stellar masses imply that the assemblage of these galaxies took place at the same time as the initial burst of star formation. This result leads us to conclude that dry merging has had little effect on the average stellar mass of BCGs over the last 9–10 Gyr in stark contrast to the predictions of semi-analytic models, based on the hierarchical merging of dark matter halos, which predict a more protracted mass build-up over a Hubble time. However, we discuss that there is potential for reconciliation between observation and theory if there is a significant growth of material in the intracluster light over the same period.

Key words: galaxies: clusters: general – galaxies: evolution – galaxies: elliptical and lenticular, cD

Online-only material: color figures

1. INTRODUCTION

Brightest Cluster Galaxies (BCGs) are the most luminous objects in the universe in terms of stellar light and appear to be a separate population from bright ellipticals (Sandage 1972, 1976; Bhavsar & Barrow 1985; Oegerle & Hoessel 1991; Postman & Lauer 1995; Bernstein & Bhavsar 2001; Bernardi et al. 2007; von der Linden et al. 2007; Vale & Ostriker 2008; Lin et al. 2010). They reside in the deep potential wells of the cores of rich galaxy clusters, thought to descend from the first regions where mass began to accumulate after the big bang. Their luminosities and unique environments make them ideal candidates for the testing of the mass build-up in galaxies across a large fraction of the Hubble time.

A number of studies have attempted to constrain the formation epoch and evolution of BCGs by comparing their *K*-band Hubble diagram to a range of stellar population models (e.g., Aragon-Salamanca et al. 1998; Collins & Mann 1998; Nelson et al. 2002). BCGs have been shown to follow passive evolution out to moderate redshifts but then differing results are seen at $z > 0.5$, with some groups seeing a continuation of the passive trend (e.g., Collins & Mann 1998), while others claim that the high redshift BCGs are fainter and therefore less massive than their local counterparts (e.g., Aragon-Salamanca et al. 1998). This is explained by a dependence of BCG luminosity on the mass of its host cluster (Burke et al. 2000), with most studies now agreeing that the evolution of BCGs in massive clusters can be described as passive to $z \sim 0.8$ (Stott et al. 2008; Whiley et al. 2008). However, there is still some debate over the recent merging activity of BCGs, particularly in lower mass clusters and Brightest Group Galaxies, with a number of studies identifying major merger candidates (Mulchaey et al. 2006; Rines et al. 2007; Tran et al. 2008).

The favored model for galaxy formation and evolution is via the hierarchical merging of dark matter halos (e.g., Davis et al. 1985). In this model, the mass of a galaxy gradually increases as it merges with neighboring systems. A major development in the field has been the advent of large cosmological simulations such as the Millennium *N*-body Simulation (Springel et al. 2005) which models this hierarchical mass build-up of dark matter halos in a comoving box 500 h^{-1} Mpc (where $h = H_0/100\,\mathrm{km\,s^{-1}\,Mpc^{-1}}$) on the side.

Semi-analytic models are commonly used to describe the complex baryonic physics of galaxies in the context of the merger histories of dark matter halos within *N*-body simulations (e.g., Bower et al. 2006; De Lucia & Blaizot 2007). These

models are an efficient way to describe the competing processes affecting baryonic matter such as those that trigger or suppress star formation, i.e., gas-rich galaxy merging and feedback from active galactic nuclei or supernovae. The output of observables, such as galaxy magnitudes, from the semi-analytic models has proved to be valuable for astronomers as the modeled systems can be compared directly with measurable quantities. For this reason semi-analytic models can be a useful tool for making mock catalogs, predicting the behavior of galaxies, testing cosmological theory, and assessing the feasibility of telescope observations.

One important advantage of using BCGs to study galaxy evolution is that their theoretical counterparts can be easily and unambiguously identified as the central massive galaxies in mock clusters at the same redshift as the real systems. De Lucia & Blaizot (2007) presented the evolution of BCGs over a Hubble time, in a semi-analytic model based on the Millennium Simulation. This paper predicted that the stellar population of BCGs forms early, with 50% of the stellar mass in place by $z = 5$ and 80% by $z = 3$. However, this early star formation takes place in separate components that gradually assemble into the BCGs seen in the local universe, mainly through dry mergers that do not trigger additional star formation. So, for example, at $z = 1.5$ the sum of the stellar mass in all sub-components is over 90% of the mass of the fully assembled BCG at $z = 0$, whereas the stellar mass in the main progenitor is on average only 20% of the galaxy's final mass.

From an observational standpoint, a significant number of high redshift galaxy clusters ($z \gtrsim 1$) have been discovered in recent years with X-ray surveys (e.g., Rosati et al. 2004; Mullis et al. 2005; Stanford et al. 2006; Bremer et al. 2006; Lamer et al. 2008). The *XMM* Cluster Survey (XCS; Romer et al. 2001; Sahlén et al. 2009) is one such project performing a serendipitous survey to discover clusters in the *XMM-Newton* archive. The main goals of the XCS are to constrain cosmological parameters, measure the evolution of the hot gas through analysis of the cluster scaling relations, and study galaxy evolution in clusters since the high-mass cluster cores are thought to be environments comparable across all epochs. Furthermore, X-ray luminosity and temperature are excellent proxies of cluster mass and enable us to directly compare the properties of real cluster galaxies with mock galaxies in similar cluster halo environments. With the advent of large wide-field optical and infrared surveys it is also possible to photometrically select high redshift galaxy clusters based on the properties of their constituent galaxies, further increasing the number of known $z > 1$ clusters (e.g., Barrientos et al. 2004; Swinbank et al. 2007; Eisenhardt et al. 2008).

In this paper, we present near-infrared observations of 20 high redshift galaxy clusters ($0.8 < z < 1.5$), derive stellar masses for their BCGs, and compare them with the latest semi-analytic models based on the Millennium *N*-body Simulation (De Lucia & Blaizot 2007; Springel et al. 2005). We test how robust our results are against different star formation histories produced by three independent stellar population codes: Bruzual & Charlot (2003), Maraston (2005), and BaSTI (Pietrinferni et al. 2004; Percival et al. 2009). This work builds on the result of Collins et al. (2009), in which we found that the average stellar mass of the BCGs in five of the highest redshift galaxy clusters is not significantly different to that of BCGs in the local universe.

Unless otherwise stated a Lambda Cold Dark Matter (ΛCDM) cosmology (Ω_M =0.3, $\Omega_{\rm Vac} = 0.7$, H_0 =70 km s^{-1} Mpc^{-1}) is used throughout this work.

2. CLUSTER SAMPLE

Table 1 details our sample of 20 of the most distant, spectroscopically confirmed, galaxy clusters, including the highest redshift X-ray selected cluster XMMXCS J2215.9−1738 (Stanford et al. 2006; Hilton et al. 2007, 2009). The sample consists of clusters discovered by various X-ray surveys and several selected by optical methods that show extended X-ray emission (see Table 1). All the clusters have spectroscopically confirmed redshifts in the range $0.8 \lesssim z \lesssim 1.5$ and X-ray luminosities of $1 \lesssim L_X \lesssim 19 \times 10^{44}$ erg s^{-1}.

To anchor our analysis to the local universe we also include a low redshift comparison sample ($0 \lesssim z \lesssim 0.3$, $0.7 \lesssim L_X \lesssim 20.0 \times 10^{44}$ erg s^{-1}) published in Stott et al. (2008). This sample is a good low redshift comparison as the clusters cover a similar range in mass (average mass at $z < 0.1$ is $6.8(\pm1.5) \times 10^{14} M_\odot$) to the low redshift halos of the Millennium Simulation (average mass at $z = 0$ is $7.5(\pm3.5) \times 10^{14} M_\odot$).

2.1. Cluster Mass

A number of authors have identified a weak correlation between BCG mass and their host cluster mass (Edge 1991; Collins & Mann 1998; Burke et al. 2000; Brough et al. 2008; Stott et al. 2008; Whiley et al. 2008) which does not change significantly with redshift out to $z \simeq 0.8$. Therefore, in order to compare measured and predicted BCG masses in a meaningful way, it is necessary that our cluster sample be well matched to the masses of simulated clusters in the Millennium Simulation with which we are comparing. The clusters of interest from the simulation are the 125 most massive systems in the redshift snapshots $z = 0.76$, $z = 1.08$, and $z = 1.5$, selected for comparison with observations (De Lucia & Blaizot 2007). Halo masses M_{200} are measured at a radius (R_{200}) inside which the average mass density is 200 times the critical density of the universe.

We calculate M_{200} and the associated uncertainties of our sample based on the observational results for the mass–temperature (M–T_X) relation, which is preferable to the L_X-based determinations used in Collins et al. (2009) due to the putative presence of cluster cooling cores. The cluster X-ray temperatures used are listed in Table 1. We parameterize the M–T_X relation as

$$\left(\frac{M_{500}}{10^{14}\,M_\odot}\right) = M_* \left(\frac{T_X}{1\,\mathrm{keV}}\right)^{\alpha} E^{\beta}(z)\,, \qquad (1)$$

with a log-normal scatter $N(0, \sigma_{\log T})$. Here, $E(z)$ is the standard Hubble parameter at redshift z. The M_{500} masses are converted to M_{200} using the standard Navarro–Frenk–White-profile prescription by Hu & Kravtsov (2003) with a halo concentration parameter $c = 5$. We include a $\sigma = 10\%$ uncertainty on the normalization M_* (similar to typical expected uncertainties in mass estimation; e.g., Nagai et al. 2007) along with the estimated measurement uncertainties on the temperatures, and from these derive the uncertainties on the M_{200} values by a simple Monte Carlo simulation.

We use the parameter values based on the Maughan (2007) derived M–T_X relation, using the "center excluded" estimates in their Table 1:

$$\log_{10}(M_*) = -0.57,\ \alpha = 1.72,\ \beta = -0.82,\ \sigma_{\log T} = 0.06.$$

This normalization agrees with the relatively well-established value $M_{500}(z = 0.05, T_X = 5\,\mathrm{keV}) \approx 3 \times 10^{14} h^{-1} M_\odot$; e.g., Pierpaoli et al. (2001), Reiprich & Böhringer (2002), Viana et al.

Table 1
The Cluster Sample

Cluster	R.A. (J2000)	Decl. (J2000)	z	T_X (keV)	Cluster Mass $10^{14}(M_\odot)$	BCG m_{K_s}	BCG Stellar Mass[a] $10^{12}(M_\odot)$	T_X Reference
1. CL J0152.7−1357	01h52m41s	−13d57m45s	0.83	$5.4^{+0.9}_{-0.9}$	$4.5^{+2.7}_{-2.2}$	16.96 ± 0.08	0.58 ± 0.11	Vikhlinin et al. (2009)
2. XLSS J022303.0−043622[b]	02h23m53.9s	−04d36m22s	1.22	$3.5^{+0.4}_{-0.4}$	$1.8^{+0.9}_{-0.7}$	17.72 ± 0.01	0.61 ± 0.08	Bremer et al. (2006)
3. XLSS J022400.5−032526[b]	02h24m00s	−03d25m34s	0.81	$3.6^{+0.4}_{-0.4}$	$2.3^{+1.4}_{-0.8}$	16.49 ± 0.10	0.85 ± 0.18	Andreon et al. (2005)
4. RCS J0439−2904	04h39m38s	−29d04m55s	0.95	$1.5^{+0.3}_{-0.2}$	$0.5^{+0.4}_{-0.2}$	17.70 ± 0.08	0.40 ± 0.07	Hicks et al. (2008)
5. 2XMM J083026+524133	08h30m25.9s	52d41m33s	0.99	$8.2^{+0.9}_{-0.9}$	$8.5^{+4.1}_{-3.4}$	16.58 ± 0.05	1.24 ± 0.22	Lamer et al. (2008)
6. RX J0848.9+4452[c]	08h48m56.3s	44d52m16s	1.26	$6.2^{+1.0}_{-0.9}$	$4.7^{+2.8}_{-2.0}$	17.00 ± 0.02	1.30 ± 0.15	Balestra et al. (2007)
7. RDCS J0910+5422	09h10m44.9s	54d22m09s	1.11	$6.4^{+1.5}_{-1.2}$	$5.3^{+4.1}_{-2.5}$	17.88 ± 0.05	0.48 ± 0.08	Balestra et al. (2007)
8. CL J1008.7+5342	10h08m42s	53d42m00s	0.87	$3.6^{+0.8}_{-0.6}$	$2.2^{+1.6}_{-1.0}$	16.42 ± 0.08	1.06 ± 0.21	Maughan et al. (2006)
9. RX J1053.7+5735 (West)	10h53m39.8s	57d35m18s	1.14	$4.4^{+0.3}_{-0.3}$	$2.7^{+1.4}_{-1.0}$	17.21 ± 0.06	1.03 ± 0.19	Hashimoto et al. (2004)
10. MS1054.4−0321	10h57m00.2s	−03d37m27s	0.82	$7.8^{+1.0}_{-0.9}$	$8.5^{+4.9}_{-3.2}$	16.04 ± 0.10	1.35 ± 0.29	Branchesi et al. (2007)
11. CL J1226+3332	12h26m58s	33d32m54s	0.89	$10.6^{+1.1}_{-1.1}$	$13.9^{+6.6}_{-5.4}$	16.00 ± 0.06	1.66 ± 0.31	Maughan et al. (2004)
12. RDCS J1252.9−2927	12h52m54.4s	−29d27m17s	1.24	$7.2^{+0.4}_{-0.6}$	$6.1^{+2.3}_{-2.4}$	17.36 ± 0.03	0.89 ± 0.11	Balestra et al. (2007)
13. RDCS J1317+2911	13h17m21.7s	29d11m18s	0.81	$4.0^{+1.3}_{-0.8}$	$2.7^{+2.9}_{-1.3}$	17.27 ± 0.15	0.41 ± 0.10	Branchesi et al. (2007)
14. WARPS J1415.1+3612	14h15m11.1s	36d12m03s	1.03	$6.2^{+0.8}_{-0.7}$	$5.2^{+2.9}_{-1.9}$	16.76 ± 0.04	1.15 ± 0.19	Branchesi et al. (2007)
15. CL J1429.0+4241	14h29m06.4s	42d41m10s	0.92	$6.2^{+1.5}_{-1.0}$	$5.5^{+5.3}_{-2.0}$	17.43 ± 0.20	0.47 ± 0.13	Maughan et al. (2006)
16. CL J1559.1+6353	15h59m06s	63d52m60s	0.85	$4.1^{+1.4}_{-1.0}$	$2.8^{+3.2}_{-1.5}$	17.21 ± 0.09	0.49 ± 0.10	Maughan et al. (2006)
17. CL 1604+4304	16h04m25.2s	43d04m53s	0.90	$2.5^{+1.1}_{-0.7}$	$1.2^{+1.6}_{-0.6}$	17.61 ± 0.09	0.38 ± 0.07	Lubin et al. (2004)
18. RCS J162009+2929.4	16h20m09.4s	29d29m26s	0.87	$4.6^{+2.1}_{-1.1}$	$3.4^{+5.5}_{-1.4}$	17.63 ± 0.12	0.35 ± 0.07	Bignamini et al. (2008)
19. XMMXCS J2215.9−1738[d]	22h15m58.5s	−17d38m03s	1.46	$4.1^{+0.6}_{-0.9}$	$2.1^{+1.9}_{-0.8}$	18.72 ± 0.01	0.39 ± 0.05	Stanford et al. (2006)
20. XMMU J2235.3−2557	22h35m20.6s	−25d57m42s	1.39	$8.6^{+1.3}_{-1.2}$	$7.7^{+4.4}_{-3.1}$	17.34 ± 0.01	1.26 ± 0.14	Rosati et al. (2009)

Notes.
[a] The stellar mass errors quoted include the photometric error but not the uncertainty in the stellar population (see Section 4.2 for a full treatment).
[b] Based on *XMM* archival data analyzed by XCS (Sahlén et al. 2009).
[c] Archival photometry (Yamada et al. 2002).
[d] Based on X-ray analysis in Hilton et al. (2010).

(2003), and Vikhlinin et al. (2006). The scatter is the same as in Mantz et al. (2009), which is consistent with Maughan (2007) although the latter does not derive the M–T_X scatter explicitly.

Finally, we note that cluster mass estimates based on the somewhat steeper M–T_X relation by Mantz et al. (2009) give similar results.

Crucially, these cluster masses cover the range of massive halos seen in the equivalent redshift snapshots of the Millennium Simulation. The De Lucia & Blaizot (2007) simulated cluster samples at $z = 0.76$, $z = 1.08$, and $z = 1.5$ have mass ranges at these redshifts of 2.4–13.6 $\times$ 10^{14} $M_\odot$, 1.5–9.8 $\times$ 10^{14} $M_\odot$, and 1.0–7.5 $\times$ 10^{14} $M_\odot$, respectively. The average mass of the combined high redshift simulated halos is 2.6 ($\pm$0.1) $\times$ 10^{14} $M_\odot$, compared to the average mass for our sample of 4.5 ($\pm$0.7) $\times$ 10^{14} $M_\odot$. However, based on the known trend of BCG mass with M_{200} (see Section 4.1), this 60% difference in average cluster mass equates at most to a shift in the average BCG mass of around 10%, which is within the measurement uncertainties. The consequences of this mismatch in cluster mass between the high redshift observations and the simulation are discussed in Section 4.3.

3. OBSERVATIONS AND DATA REDUCTION

The observations were taken with the MOIRCS camera (Ichikawa et al. 2006) on the 8.2 m Subaru telescope which provides imaging and low-resolution spectroscopy over a total field of view of 4′ $\times$ 7′ with a pixel scale of 0.″117 pixel^{-1}. This is achieved by dividing the Cassegrain focal plane and then refocusing the light through identical optics onto two HAWAII-2 2048 $\times$ 2048 CCDs, each covering 4′ $\times$ 3.′5. Observations were taken in 0.″5 seeing on the nights of 2007 August 8 and 9 and in 0.″3–0.″6 seeing on the nights of 2008 December 16 and 2009 April 18 with the clusters centered on Detector 2. A circular 11-point dither pattern of radius 25″ was used for both bands to ensure good sky subtraction. The modal integration times were 25 minutes at J and 21 minutes at K_s although we observed some of the higher redshift clusters for 50% longer when scheduling allowed. These exposures reach a 5σ limiting magnitude of at least $J \simeq 22.5$ and $K_s \simeq 21.5$ (Vega).

The data were reduced using the external IRAF package MCSRED. The data were flat-fielded, sky subtracted, corrected for distortion caused by the camera optical design, and registered to a common pixel coordinate system. The final reduced images on which we performed the photometry were made by taking the 3σ (s.d.) clipped mean of the dither frames. The BCG photometry was extracted in an identical manner to the low redshift comparison sample from Stott et al. (2008) using SExtractor (ver. 2.5) MAG_AUTO magnitude, which is found to be within ∼0.1 mag of the total for extended objects (Martini 2001). As a test of this method we also performed large aperture (50 kpc) photometry on the BCGs finding the values to be consistent with those of MAG_AUTO to within 0.05 mag. This ability to exclude light from close neighbors by using MAG_AUTO ensures that we are not including additional flux that would bias our stellar masses to higher values. We choose a global photometric background over a local one to control for any bias introduced by a low surface brightness halo or intracluster light in the vicinity of the BCG. To calculate the colors of the BCGs the images are first matched for seeing using the IRAF task PSFMATCH; then we run SExtractor in the dual image mode so that the K_s-band detections extract the J-band catalog with identical positions and apertures to ensure accurate color determination. This photometry is performed within fixed 8 kpc circular apertures at the cluster redshift.

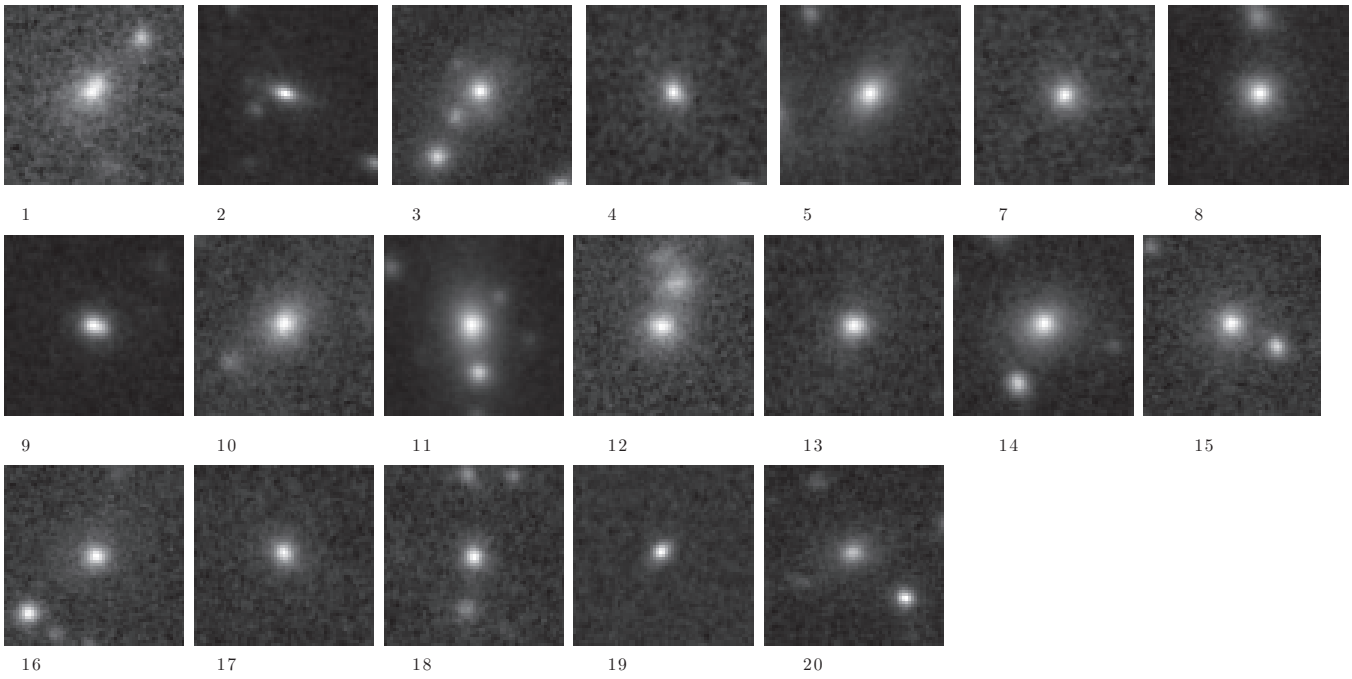

Figure 1. 7 × 7 arcsec postage stamp K_s-band images of our 19 Subaru MOIRCS observed BCGs numbered as in Table 1. RX J0848.9+4452 is absent as this is an archival BCG (Yamada et al. 2002) for which we do not possess Subaru MOIRCS imaging.

The photometry was calibrated to the Vega system using a combination of standard star observations and the Two Micron All Sky Survey and UKIDSS catalogs. The typical photometric errors are 0.01 and 0.08 for the standard star and survey calibrated data, respectively.

Additional archival BCG photometry is included for the cluster RX J0848.9+4452 (Yamada et al. 2002) which is a total K_s magnitude measured with a large aperture and is thus comparable to our own photometric analysis.

3.1. BCG Selection

The BCG selection for a cluster is usually obvious from visual inspection of the images, as for such rich clusters they are the prominent galaxy closest to the X-ray centroid often with a cD-like profile; however, we chose to formalize this by studying the tip of the red sequence in the color–magnitude relation. For each cluster we identified the red sequence with $J-K_s$ color and selected the brightest galaxy from the K_s-band magnitudes of all the red sequence galaxies within a projected distance of 500 kpc from the cluster X-ray centroid, as for approximately 95% of clusters the BCG lies within this radius (Lin & Mohr 2004). The only non-obvious case is J2215.9−1738 where the object identified as the BCG is a spectroscopically confirmed member lying 300 kpc from the X-ray centroid which is only marginally brighter than several others in the cluster. A full discussion of this identification and the properties of other candidates is presented in Hilton et al. (2009). K_s-band images of our high redshift BCGs are shown in Figure 1.

4. STELLAR MASS

4.1. Initial Stellar Mass Calibration

To compare the stellar mass build-up in our observed BCGs with those of the semi-analytic model we need to derive stellar mass from the K_s-band luminosity of the galaxies. We first do this by calculating absolute K_s-band magnitudes for our galaxies by choosing a model appropriate to the stellar population of the modeled BCGs. The De Lucia & Blaizot (2007) semi-analytic model predicts a star formation history for the BCGs in which 50% of the stars have formed by $z = 5$ and 80% by $z = 3$, albeit in separate components that have not yet coalesced to form the final mass of the galaxy. To model this evolution a stellar population from Bruzual & Charlot (2003) with a Chabrier (2003) initial mass function (IMF) is implicit in the semi-analytic model. In Figure 2, we investigate the stellar population of our observed BCG sample by plotting the $J - K_s$ color against redshift and comparing to two Bruzual & Charlot (2003) simple stellar population (SSP) models with a Chabrier IMF and solar metallicity. A composite stellar population (CSP) with an exponentially decaying star formation rate with $\tau = 0.9$ Gyr which mimics the average stellar population present in the simulation (i.e., 50% of the stars have formed by $z = 5$ and 80% by $z = 3$) is also plotted. From this plot, we can see that although there is some scatter in the BCG near-infrared colors at $z \sim 1$ they are consistent with the CSP model. It should be stressed that this color evolution only gives information about the stellar population (e.g., age and metallicity) and not the mass of the system.

With the initial assumption that our observed BCGs have similar stellar populations to those of De Lucia & Blaizot (2007), we calculate their stellar masses using the mass-to-light ratios from the CSP and normalize these masses and the model BCG masses from De Lucia & Blaizot (2007) at $z = 0$. We discuss the consequences of this assumption in Section 4.2 and compare a larger set of stellar population models appropriate to our BCGs.

By using this technique we find stellar masses for our BCGs in the range 3.45–16.63 × $10^{11}\,M_{\odot}$ with a biweight scale value of 8.52(±1.00) × $10^{11}\,M_{\odot}$ which is consistent with the local BCG mass of 8.99(±0.82) × $10^{11} M_{\odot}$. So, when considering our entire sample with stellar masses derived directly from the CSP model, we find that on average there has been no significant change in the stellar mass of BCGs out to at least $z = 1.5$. The corresponding stellar masses

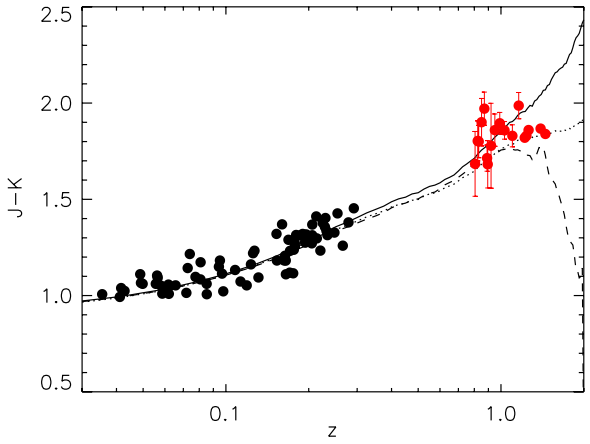

Figure 2. $J - K_s$ color vs. redshift for our high redshift sample (red) with 1σ error bars and the low redshift analog sample of Stott et al. (2008, black). Two Bruzual & Charlot (2003) solar metallicity SSP models are included with formation redshifts $z_f = 2$ (dashed) and $z_f = 5$ (solid) as well as the model chosen to mimic the star formation histories of the De Lucia & Blaizot (2007) semi-analytic model which forms 50% of its stars by $z = 5$ and 80% by $z = 3$ (dotted).

(A color version of this figure is available in the online journal.)

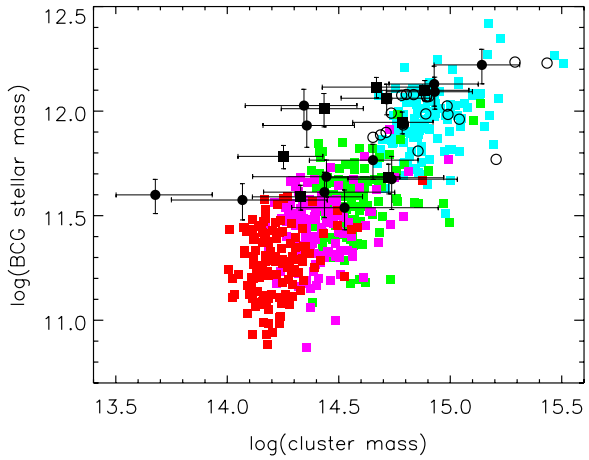

Figure 3. BCG stellar mass ($M_\odot$) vs. cluster mass ($M_\odot$) for our sample (filled black circles $z < 1$ and filled black squares $z > 1$ to demonstrate that there is no redshift dependence). The error bars in the cluster mass include both the X-ray observation and full mass–temperature scaling errors, whereas the stellar mass errors include the photometric errors, not the uncertainty in the stellar population; see Section 4.2 and Figure 4. The colored squares represent the BCGs from the model of De Lucia & Blaizot (2007) at the redshift snapshots $z = 0$, 0.76, 1.0, and 1.5 (cyan, green, pink, and red). The open circles show the $z < 0.1$ BCGs from the low-z comparison sample of Stott et al. (2008).

(A color version of this figure is available in the online journal.)

from the simulation at $z = 0.76$, 1.08, and 1.5 are respectively 3.84 ± 0.14, 2.91 ± 0.10, and 1.92 ± 0.07 in units $10^{11}\ M_\odot$. The results of this analysis can be seen in Figure 3 in which we plot stellar mass versus cluster mass for our BCG sample (black filled) and those of De Lucia & Blaizot (2007) at four different redshift snapshots ($z = 0$, 0.76, 1.0, and 1.5 corresponding to cyan, green, pink, and red squares, respectively). From this plot, it is clear that the average mass of the observed BCGs is significantly higher than that of the model BCGs for clusters of similar mass and redshift.

We note here that the choice of the semi-analytic model does not affect our results as the "Durham models" (i.e., Bower et al. 2006) also give a near identical discrepancy to that seen here (Collins et al. 2009).

From Figure 3, we see that the highest mass BCG is found in the highest mass cluster which may suggest a link between stellar mass and environment as seen by Edge (1991), Collins & Mann (1998), Brough et al. (2008), Stott et al. (2008), and Whiley et al. (2008). However for our sample of 20, the correlation between BCG mass ($M_{\rm BCG}$) and M_{200} is weak with a power-law exponent of 0.42 ± 0.12 and Spearman's rank analysis indicating this correlation is significant to the 99% level. Determination of this correlation in the literature from larger samples at lower redshift typically show a small dependence; for example, Whiley et al. (2008) find a power-law exponent of 0.12 ± 0.03, with Spearman's rank correlation significant to greater than the 99.9% level. However, as mentioned in Section 2.1 it is clear from Figure 3 that there is some mismatch in cluster mass between the high redshift clusters and the corresponding simulated halos; we discuss the effect of this in Section 4.3.

4.2. Dependence on Stellar Population Models

Rather than relying on the potentially naive stellar mass calibration used in Section 4.1 we look now at a range of stellar population models and codes with physically motivated input parameters to study their effects on the stellar mass evolution result. For completeness we utilize three leading independent stellar population codes in this analysis, namely Bruzual & Charlot (2003), Maraston (2005), and BaSTI (Pietrinferni et al. 2004; Percival et al. 2009), all of which are now widely used for extragalactic astronomy. In Collins et al. (2009) we investigated mass-to-light ratios extensively at $z = 1.3$ and found that our result held for the majority of combinations of stellar population synthesis code, age, and metallicity. The notable exception to this was for young and sub-solar metallicity SSPs generated by the code of Maraston (2005) which, because of a strong emphasis on the asymptotic giant branch phase of stellar evolution, gives young stellar populations ($\sim$1 Gyr) red colors degenerate with old age and high metallicity models.

Until recently reliable metallicity determinations were available for only a few local BCGs. However, Loubser et al. (2009) examined the stellar populations of 49 BCGs in the local universe with high signal-to-noise spectra, concluding that on average they have at least twice-solar metallicity ($[Z/{\rm H}] = 0.31 \pm 0.17$) and enhanced α elements ($[E/{\rm Fe}] = 0.41 \pm 0.09$), suggesting an intense burst of star formation and subsequent quiescence. We use this information to rule out the low metallicity models and repeat the mass-to-light ratio analysis of Collins et al. (2009), concentrating on the variation in the age of the stellar component at twice-solar metallicity and including α enhancement (available only for BaSTI). Due to the differing metallicity sampling and IMFs available for the three stellar population codes, we use Bruzual & Charlot (2003) with $2.5\,Z_\odot$ and Chabrier IMF (Chabrier 2003); Maraston (2005) with $2.2\,Z_\odot$ and Kroupa IMF (Kroupa 2001); and BaSTI with $2.0\,Z_\odot$ and Kroupa IMF. We calculate the mass-to-light ratios derived from these models for galaxies at the average redshift of our sample $z = 1.0$ and ages corresponding to formation redshifts $2 < z_f < 5$ (2.6–4.7 Gyr at $z = 1$). The results of this analysis can be seen in Figure 4, with the Bruzual & Charlot (2003) models giving the highest stellar masses followed by BaSTI (scaled solar then α enhanced) and the Maraston (2005) models giving the lowest. The average stellar mass predicted by the semi-analytic model at $z = 1.0$ is $2.91(\pm 0.10) \times 10^{11} M_\odot$. Therefore, results of the mass-to-light ratio analysis have 3σ

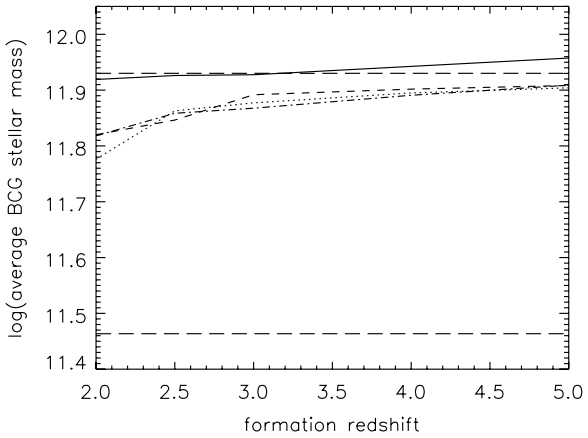

Figure 4. Average stellar mass ($M_\odot$) vs. formation redshift for our high redshift BCG sample when using mass-to-light ratios derived from three stellar population codes: Bruzual & Charlot (2003), BaSTI (Pietrinferni et al. 2004; Percival et al. 2009) scaled solar, BaSTI α enhanced and Maraston (2005) (solid, short dashed, dot-dashed, and dotted lines respectively) with fixed twice-solar metallicity, evaluated at the average redshift of our sample ($z = 1.0$). The upper long dashed line represents the average local BCG stellar mass $8.99 \pm 0.82 \times 10^{11} M_\odot$, while the lower long dashed line represents the average stellar mass of the De Lucia & Blaizot (2007) semi-analytic model at $z = 1$ ($2.91 \pm 0.10 \times 10^{11} M_\odot$).

significance or greater for all stellar population models considered here. This confirms that our result from Section 4.1 is robust to the influence of reasonable, physically motivated, star formation histories generated by independent synthesis codes.

4.3. Dependence on Cluster Mass

Due to the nature of detecting high redshift clusters in flux-limited X-ray surveys, the clusters in our sample are relatively high mass systems. Because of this there is some mismatch between the average cluster mass of our sample and the average halo masses of the simulation (see Section 2.1). Given the relationship between cluster mass and BCG mass, previously discussed, this may lead to an unfair comparison. To account for this we perform a bootstrap simulation using the observations and the Millennium Simulation halos. The details of this simulation are as follows: we select a cluster at random from our observed sample, we then pick a model BCG from a halo of similar mass to the observation using a random normal selection with a sigma equivalent to the error on the X-ray inferred cluster mass as listed in Table 1. To account for the discrete nature of the simulated redshifts we interpolate the model BCG stellar mass to the redshift of the observed cluster. This procedure is repeated 10,000 times allowing for replacement. The resulting distribution has an average stellar mass of $3.9 \pm 0.2 \times 10^{11} M_\odot$ which is $\sim 5\sigma$ away from the average mass of our sample, $8.52(\pm 1.00) \times 10^{11} M_\odot$. Thus, the significance of our result does not decrease when cluster selection effects are accounted for.

5. SUMMARY AND DISCUSSION

We have demonstrated that the average stellar mass of BCGs in the highest redshift X-ray clusters is discrepant with those from similar mass dark matter halos in semi-analytic models based on the Millennium Simulation. Instead of the gradual build-up of mass through dry merging predicted by De Lucia & Blaizot (2007), our observations suggest that the stellar mass in these objects has remained unchanged over the last 9–10 Gyr requiring a more rapid build-up of stellar mass before $z = 1.5$, some 4–5 Gyr after the big bang.

The timescale for the mass assemblage is similar to the age of the component stars (2–3 Gyr), a situation that appears to resemble classical monolithic collapse (Eggen et al. 1962; Larson 1974) rather than hierarchical formation. To form a galaxy of stellar mass 10^{12} $M_\odot$ over 4 Gyr requires a mass deposition rate of about 250 $M_\odot$ yr^{-1} and an efficient mechanism to feed the gas into the inner regions of the halo where it can form stars. Unfortunately the merging process becomes inefficient for massive galaxies because merger-induced shocks lead to heating as opposed to radiative cooling of the gas (Binney 2004). One suggestion is that the early assembly of massive galaxies at $z \geqslant 2$ is driven by narrow streams of dense cold gas which penetrate the shock-heated region greatly increasing the efficiency of the gas deposition and associated star formation (Birnboim & Dekel 2003; Kereš et al. 2005; Dekel et al. 2009).

Alternatively, a deficiency may lie in the semi-analytic treatment of the physical processes in the densest environments during early hierarchical assembly; this contention is supported by the fact that current predictions are moderately consistent with observations of the evolution of luminous red galaxies (Wake et al. 2006; Almeida et al. 2008), whereas our results, which focus on the most massive subset of this population, the BCGs, differ much more from the model predictions.

From a theoretical point of view this area of research is constantly evolving due to the challenges posed by observation and the increased availability of powerful computers. A recent high resolution simulation of a single cluster (Ruszkowski & Springel 2009) predicts that 50% of the BCG final mass in a massive ($10^{15} M_\odot$) cluster has built up by hierarchical merging in the last nine billion years, decreasing the discrepancy between our findings and theory. As this is for one cluster and not a full cosmological simulation on the scale of the Millennium Simulation it is difficult to know whether this improvement is due to low number statistics or a better approximation of *N*-body and stellar-dynamical effects.

One consequence of our result is that if merging is important at all since $z \simeq 1$, the evolution of BCGs must be dominated by minor rather than major mergers, since the stellar mass appears unchanged since this time. Our observations are broadly consistent with the relatively low number of dry major mergers found at low redshift (Liu et al. 2009) and the model predictions of Khochfar & Silk (2009) which show that only 10%–20% of galaxies more massive than $6.3 \times 10^{10} M_\odot$ have experienced dry major mergers within their last Gyr at any given redshift $z \leqslant 1$. Numerical simulations find that the scale sizes of early galaxies can grow from dry minor merging by a factor of 2–3 since $z = 1$, e.g., Naab et al. (2009), and suggest that the cD-like halos of BCGs are formed late, resulting in the relatively recent departure of BCGs from the Kormendy relation for ordinary elliptical galaxies (Ruszkowski & Springel 2009).

One possibility which might help reconcile observations and theory is the growth of stellar material constituting the diffuse intracluster light within the cluster cores. From dissipationless simulations of dark matter halos, Conroy et al. (2007b) find that while BCGs do not appear to evolve strongly at $z < 1$, the intracluster light surrounding such galaxies grows substantially, with up to $\sim$85% of the stars in the intracluster medium of present-day clusters deposited at $z < 1$ (see also Willman et al. 2004; Murante et al. 2007; Conroy et al. 2007a; White et al. 2007; Henriques & Thomas 2010). This inside-out growth is broadly consistent with the dry minor merging scenario for the

local elliptical galaxy population (Bezanson et al. 2009; Hopkins et al. 2010) required to explain their rapid size increase since $z \sim 2$ (van Dokkum et al. 2009, 2010).

Observationally, recent results have confirmed the overall importance of intracluster light: Rudick et al. (2006) find that the intracluster light constitutes ∼10% of the entire cluster stellar light, a result that appears to hold even for non-cD clusters (Feldmeier et al. 2004). From surface photometry out to 300 kpc of 24 clusters at $z < 0.1$, Gonzalez et al. (2005) demonstrate that the outer cD component of BCGs traces the cluster potential and has ∼10 times the total luminosity of the inner elliptical profile. These results suggest that further work on the growth of stellar light in the outer parts of BCGs is required to provide a consensus.

First, we thank the anonymous referee for their useful comments which have improved the clarity of this paper.

We acknowledge financial support from Liverpool John Moores University and the STFC. M.H. acknowledges support from the South African National Research Foundation. M.S. acknowledges financial support from the Swedish Research Council (VR) through the Oskar Klein Centre for Cosmoparticle Physics. P.T.P.V. acknowledges financial support from FCT project PTDC/CTE-AST/64711/2006.

We thank Gabriella De Lucia for making simulation results available to us in tabular form, Ichi Tanaka for developing the MCSRED package used to reduce the MOIRCS data, Maurizio Salaris for discussions on stellar population synthesis models, and Ben Maughan for discussions on cluster masses.

This work is based in part on data collected at the Subaru Telescope, which is operated by the National Astronomical Observatory of Japan and the *XMM-Newton*, an ESA science mission funded by contributions from ESA member states and from NASA.

This publication makes use of data products from the Two Micron All Sky Survey, which is a joint project of the University of Massachusetts and the Infrared Processing and Analysis Center/California Institute of Technology, funded by the National Aeronautics and Space Administration and the National Science Foundation.

This work is based in part on data obtained as part of the UKIRT Infrared Deep Sky Survey.

The Millennium Simulation databases used in this paper and the Web application providing online access to them were constructed as part of the activities of the German Astrophysical Virtual Observatory.

IRAF is distributed by the National Optical Astronomy Observatories, which are operated by the Association of Universities for Research in Astronomy, Inc., under cooperative agreement with the National Science Foundation.

REFERENCES

Almeida, C., Baugh, C. M., Wake, D. A., Lacey, C. G., Benson, A. J., Bower, R. G., & Pimbblet, K. 2008, MNRAS, 386, 2145
Andreon, S., Valtchanov, I., Jones, L. R., Altieri, B., Bremer, M., Willis, J., Pierre, M., & Quintana, H. 2005, MNRAS, 359, 1250
Aragon-Salamanca, A., Baugh, C. M., & Kauffmann, G. 1998, MNRAS, 297, 427
Balestra, I., Tozzi, P., Ettori, S., Rosati, P., Borgani, S., Mainieri, V., Norman, C., & Viola, M. 2007, A&A, 462, 429
Barrientos, L. F., Gladders, M. D., Yee, H. K. C., Infante, L., Ellingson, E., Hall, P. B., & Hertling, G. 2004, ApJ, 617, L17
Bernardi, M., Hyde, J. B., Sheth, R. K., Miller, C. J., & Nichol, R. C. 2007, AJ, 133, 1741
Bernstein, J. P., & Bhavsar, S. P. 2001, MNRAS, 322, 625
Bezanson, R., van Dokkum, P. G., Tal, T., Marchesini, D., Kriek, M., Franx, M., & Coppi, P. 2009, ApJ, 697, 1290
Bhavsar, S. P., & Barrow, J. D. 1985, MNRAS, 213, 857
Bignamini, A., Tozzi, P., Borgani, S., Ettori, S., & Rosati, P. 2008, A&A, 489, 967
Binney, J. 2004, MNRAS, 347, 1093
Birnboim, Y., & Dekel, A. 2003, MNRAS, 345, 349
Bower, R. G., Benson, A. J., Malbon, R., Helly, J. C., Frenk, C. S., Baugh, C. M., Cole, S., & Lacey, C. G. 2006, MNRAS, 370, 645
Branchesi, M., Gioia, I. M., Fanti, C., & Fanti, R. 2007, A&A, 472, 727
Bremer, M. N., et al. 2006, MNRAS, 371, 1427
Brough, S., Couch, W. J., Collins, C. A., Jarrett, T., Burke, D. J., & Mann, R. G. 2008, MNRAS, 385, L103
Bruzual, G., & Charlot, S. 2003, MNRAS, 344, 1000
Burke, D. J., Collins, C. A., & Mann, R. G. 2000, ApJ, 532, L105
Chabrier, G. 2003, PASP, 115, 763
Collins, C. A., & Mann, R. G. 1998, MNRAS, 297, 128
Collins, C. A., et al. 2009, Nature, 458, 603
Conroy, C., Ho, S., & White, M. 2007a, MNRAS, 379, 1491
Conroy, C., Wechsler, R. H., & Kravtsov, A. V. 2007b, ApJ, 668, 826
Davis, M., Efstathiou, G., Frenk, C. S., & White, S. D. M. 1985, ApJ, 292, 371
De Lucia, G., & Blaizot, J. 2007, MNRAS, 375, 2
Dekel, A., et al. 2009, Nature, 457, 451
Edge, A. C. 1991, MNRAS, 250, 103
Eggen, O. J., Lynden-Bell, D., & Sandage, A. R. 1962, ApJ, 136, 748
Eisenhardt, P. R. M., et al. 2008, ApJ, 684, 905
Feldmeier, J. J., Mihos, J. C., Morrison, H. L., Harding, P., Kaib, N., & Dubinski, J. 2004, ApJ, 609, 617
Gonzalez, A. H., Zabludoff, A. I., & Zaritsky, D. 2005, ApJ, 618, 195
Hashimoto, Y., Barcons, X., Böhringer, H., Fabian, A. C., Hasinger, G., Mainieri, V., & Brunner, H. 2004, A&A, 417, 819
Henriques, B. M. B., & Thomas, P. A. 2010, MNRAS, 403, 768
Hicks, A. K., et al. 2008, ApJ, 680, 1022
Hilton, M., et al. 2007, ApJ, 670, 1000
Hilton, M., et al. 2009, ApJ, 697, 436
Hilton, M., et al. 2010, arXiv:1005.4692
Hopkins, P. F., Bundy, K., Hernquist, L., Wuyts, S., & Cox, T. J. 2010, MNRAS, 401, 1099
Hu, W., & Kravtsov, A. V. 2003, ApJ, 584, 702
Ichikawa, T., et al. 2006, Proc. SPIE, 6269, 626916
Kereš, D., Katz, N., Weinberg, D. H., & Davé, R. 2005, MNRAS, 363, 2
Khochfar, S., & Silk, J. 2009, MNRAS, 397, 506
Kroupa, P. 2001, MNRAS, 322, 231
Lamer, G., Hoeft, M., Kohnert, J., Schwope, A., & Storm, J. 2008, A&A, 487, L33
Larson, R. B. 1974, MNRAS, 166, 585
Lin, Y.-T., & Mohr, J. J. 2004, ApJ, 617, 879
Lin, Y.-T., Ostriker, J. P., & Miller, C. J. 2010, ApJ, 715, 1486
Liu, F. S., Mao, S., Deng, Z. G., Xia, X. Y., & Wen, Z. L. 2009, MNRAS, 396, 2003
Loubser, S. I., Sanchez-Blazquez, P., Sansom, A. E., & Soechting, I. K. 2009, MNRAS, 398, 133
Lubin, L. M., Mulchaey, J. S., & Postman, M. 2004, ApJ, 601, L9
Mantz, A., Allen, S. W., Ebeling, H., Rapetti, D., & Drlica-Wagner, A. 2009, arXiv:0909.3099
Maraston, C. 2005, MNRAS, 362, 799
Martini, P. 2001, AJ, 121, 598
Maughan, B. J. 2007, ApJ, 668, 772
Maughan, B. J., Jones, L. R., Ebeling, H., & Scharf, C. 2004, MNRAS, 351, 1193
Maughan, B. J., Jones, L. R., Ebeling, H., & Scharf, C. 2006, MNRAS, 365, 509
Mulchaey, J. S., Lubin, L. M., Fassnacht, C., Rosati, P., & Jeltema, T. E. 2006, ApJ, 646, 133
Mullis, C. R., Rosati, P., Lamer, G., Böhringer, H., Schwope, A., Schuecker, P., & Fassbender, R. 2005, ApJ, 623, L85
Murante, G., Giovalli, M., Gerhard, O., Arnaboldi, M., Borgani, S., & Dolag, K. 2007, MNRAS, 377, 2
Naab, T., Johansson, P. H., & Ostriker, J. P. 2009, ApJ, 699, L178
Nagai, D., Vikhlinin, A., & Kravtsov, A. V. 2007, ApJ, 655, 98
Nelson, A. E., Gonzalez, A. H., Zaritsky, D., & Dalcanton, J. J. 2002, ApJ, 566, 103
Oegerle, W. R., & Hoessel, J. G. 1991, ApJ, 375, 15
Percival, S. M., Salaris, M., Cassisi, S., & Pietrinferni, A. 2009, ApJ, 690, 427
Pierpaoli, E., Scott, D., & White, M. 2001, MNRAS, 325, 77
Pietrinferni, A., Cassisi, S., Salaris, M., & Castelli, F. 2004, ApJ, 612, 168
Postman, M., & Lauer, T. R. 1995, ApJ, 440, 28

Reiprich, T. H., & Böhringer, H. 2002, ApJ, 567, 716
Rines, K., Finn, R., & Vikhlinin, A. 2007, ApJ, 665, L9
Romer, A. K., Viana, P. T. P., Liddle, A. R., & Mann, R. G. 2001, ApJ, 547, 594
Rosati, P., et al. 2004, AJ, 127, 230
Rosati, P., et al. 2009, A&A, 508, 583
Rudick, C. S., Mihos, J. C., & McBride, C. 2006, ApJ, 648, 936
Ruszkowski, M., & Springel, V. 2009, ApJ, 696, 1094
Sahlén, M., et al. 2009, MNRAS, 397, 577
Sandage, A. 1972, ApJ, 173, 485
Sandage, A. 1976, ApJ, 205, 6
Springel, V., et al. 2005, Nature, 435, 629
Stanford, S. A., et al. 2006, ApJ, 646, L13
Stott, J. P., Edge, A. C., Smith, G. P., Swinbank, A. M., & Ebeling, H. 2008, MNRAS, 384, 1502
Swinbank, A. M., Edge, A. C., Smail, I., Stott, J. P., Bremer, M., Sato, Y., van Breukelen, C., & Jarvis, M. 2007, MNRAS, 379, 1343
Tran, K., Moustakas, J., Gonzalez, A. H., Bai, L., Zaritsky, D., & Kautsch, S. J. 2008, ApJ, 683, L17
Vale, A., & Ostriker, J. P. 2008, MNRAS, 383, 355
van Dokkum, P. G., Kriek, M., & Franx, M. 2009, Nature, 460, 717
van Dokkum, P. G., et al. 2010, ApJ, 709, 1018
Viana, P. T. P., Kay, S. T., Liddle, A. R., Muanwong, O., & Thomas, P. A. 2003, MNRAS, 346, 319
Vikhlinin, A., Kravtsov, A., Forman, W., Jones, C., Markevitch, M., Murray, S. S., & Van Speybroeck, L. 2006, ApJ, 640, 691
Vikhlinin, A., et al. 2009, ApJ, 692, 1033
von der Linden, A., Best, P. N., Kauffmann, G., & White, S. D. M. 2007, MNRAS, 379, 867
Wake, D. A., Nichol, R. C., Eisenstein, D. J., Loveday, J., Edge, A. C., Cannon, R., Smail, I., & Schneider, D. P. 2006, MNRAS, 372, 537
Whiley, I. M., et al. 2008, MNRAS, 387, 1253
White, M., Zheng, Z., Brown, M. J. I., Dey, A., & Jannuzi, B. T. 2007, ApJ, 655, L69
Willman, B., Governato, F., Wadsley, J., & Quinn, T. 2004, MNRAS, 355, 159
Yamada, T., Koyama, Y., Nakata, F., Kajisawa, M., Tanaka, I., Kodama, T., Okamura, S., & De Propris, R. 2002, ApJ, 577, L89